

Spectra of Short Pulse Solutions of the Cubic–Quintic Complex Ginzburg–Landau Equation near Zero Dispersion

By Yannan Shen, John Zweck, Shaokang Wang, and Curtis R. Menyuk

We describe a computational method to compute spectra and slowly decaying eigenfunctions of linearizations of the cubic–quintic complex Ginzburg–Landau equation about numerically determined stationary solutions. We compare the results of the method to a formula for an edge bifurcation obtained using the small dissipation perturbation theory of Kapitula and Sandstede. This comparison highlights the importance for analytical studies of perturbed nonlinear wave equations of using a pulse ansatz in which the phase is not constant, but rather depends on the perturbation parameter. In the presence of large dissipative effects, we discover variations in the structure of the spectrum as the dispersion crosses zero that are not predicted by the small dissipation theory. In particular, in the normal dispersion regime we observe a jump in the number of discrete eigenvalues when a pair of real eigenvalues merges with the intersection point of the two branches of the continuous spectrum. Finally, we contrast the method to computational Evans function methods.

Dedicated to Mark Ablowitz, with thanks for his seminal and practical contributions to the modeling of optical fiber communications systems and short pulse lasers, and for his contagious enthusiasm. Address for correspondence: John Zweck, The University of Texas at Dallas, Department of Mathematical Sciences, FO 35, 800 West Campbell Road, Richardson, TX 75080-3021, USA; e-mail: zweck@utdallas.edu

1. Introduction

The cubic–quintic complex Ginzburg–Landau (CQ-CGL) equation provides a qualitative model for the generation of short pulses in mode-locked lasers [1]. The CQ-CGL equation includes dissipative terms that model linear filtering and nonlinear saturable gain/loss. In the special case that the dissipative terms are small, the equation is a perturbation of the cubic–quintic nonlinear Schrödinger (CQ-NLS) equation. Although the stability of solitary wave solutions of perturbed NLS equations has been extensively studied [2–4], the introduction of dissipative terms into the CQ-CGL equation gives rise to new classes of solutions. While analytical solutions to the CQ-CGL equation have been found when special relations hold between the coefficients [5–7], these solutions are unstable in the anomalous dispersion regime [8]. Moreover, in the case of large dissipative effects it has not so far been possible to prove general theorems concerning the stability of soliton solutions of the CQ-CGL equation, as was done by Kapitula and Sandstede [2,3] for the perturbed CQ-NLS equation.

In this paper, we describe computational methods to efficiently determine stationary solutions of the CQ-CGL equation as the parameters in the equation vary, to compute the spectrum of the linearization of the CQ-CGL equation about these solutions, and to compute the slowly decaying eigenfunctions that correspond to discrete eigenvalues *near the continuous spectrum*. These methods, which we discuss in Section 2, are closely related to methods developed by Wang et al. [8] to obtain stationary solutions of the Haus mode-locking equation with saturable gain and loss, and by Akhmediev and Soto-Crespo [9] and Wang et al. [8] to compute pulse spectra. Many of the theoretical results concerning the stability of solutions of nonlinear wave equations are based on an analysis of the Evans function [2,3,10–12]. Computational Evans function methods have also proved to be highly effective [13–16], and in Section 5 we contrast our approach with them.

In Section 3, we compare the results of our method to a perturbation formula of Kapitula and Sandstede [11] for an eigenvalue that bifurcates out of the edge of the continuous spectrum. Since the corresponding eigenfunction is not localized in time, this example provides an excellent test of the method. As we will explain in Section 3, this comparison highlights the importance of using a pulse ansatz for which the phase is not constant [2,3,11], but rather depends on the perturbation parameter.

In Section 4, we apply the method to study the changes that occur in the structure of the spectrum of the pulse as the dispersion is varied across

zero from the anomalous to the normal regime. To put these results into context, we first review the theoretical work of Kapitula [3] and Kapitula and Sandstede [2] who used the Evans function to analyze the discrete spectrum of the linearization of the perturbed CQ-NLS (PCQ-NLS) equation about bright solitary wave solutions. In particular, Kapitula [3] proved that, for order- ε perturbations of the CQ-NLS equation, there is an eigenvalue with multiplicity two at zero, as well as two $O(\varepsilon)$ discrete eigenvalues, at least one of which is stable. Furthermore, they showed that any other discrete eigenvalue is close to the edge of the continuous spectrum. (The continuous spectrum consists of a complex conjugate pair of half-lines in the left half of the complex plane.) In particular, if eigenvalues bifurcate from the continuous spectrum, they do so only near the edge [2].

For the parameters we used in the CQ-CGL equation, we find that in the anomalous and zero dispersion regimes (for which the dispersion parameter satisfies $D \geq 0$), the two branches of the continuous spectrum do not intersect and there are six discrete eigenvalues: two at the origin, two on the negative real axis, and two close to the edge of the continuous spectrum. Even though the dissipative terms are relatively large, this result is in qualitative agreement with the theory of Kapitula and Sandstede. On the other hand, in the normal dispersion regime, $D < 0$, the two branches of the continuous spectrum intersect at a point on the negative real axis. If D is sufficiently close to zero, there are still six discrete eigenvalues, as in the anomalous dispersion regime. However, as D decreases further, the two eigenvalues on the negative real axis merge with the intersection point of the two branches of the continuous spectrum. The theoretical results of Kapitula and Sandstede show that this last phenomenon is only possible when the dissipative terms in the CQ-CGL equation are sufficiently large. Finally, as D decreases still further below zero, the two remaining nonzero eigenvalues move away from the edge of the continuous spectrum, collide on the negative real axis, and eventually move along the negative real axis toward the right-half plane.

2. Theory and methods

2.1. Physical model

We consider the CQ-CGL equation in the form

$$iu_z + \frac{D}{2}u_{tt} + \gamma|u|^2u + \nu|u|^4u = i[\delta u + \beta u_{tt} + \epsilon|u|^2u + \mu|u|^4u], \quad (1)$$

where we have written the conservative terms on the left-hand side and the dissipative terms on the right-hand side of the equation. We model

the combined effects of loss and gain in the system using the terms with coefficients δ, ϵ , and μ . We assume that the linear loss, δ , is negative to ensure that the continuous spectrum is stable, and we model saturable nonlinear gain with a nonlinear gain coefficient, $\epsilon > 0$, and a gain saturation coefficient, $\mu < 0$. We model spectral filtering using the term with coefficient, $\beta > 0$, and the cubic and quintic nonlinear electric susceptibility of the optical fiber using the terms proportional to $\gamma > 0$ and $\nu > 0$, respectively. Finally, we recall that the chromatic dispersion coefficient, D , is positive in the anomalous or focusing dispersion regime and negative in the normal or defocusing dispersion regime.

2.2. Stationary solutions

We consider solutions of the CQ-CGL equation (1) of the form $u(t, z) = \mathcal{U}(t, z)e^{i\phi z}$, where ϕ is a constant phase and where the complex envelope, $\mathcal{U}(t, z)$, satisfies

$$\begin{aligned} \mathcal{U}_z &= (\delta - i\phi)\mathcal{U} + \left(\beta + i\frac{D}{2}\right)\mathcal{U}_{tt} + (\epsilon + i\gamma)|\mathcal{U}|^2\mathcal{U} + (\mu + i\nu)|\mathcal{U}|^4\mathcal{U} \quad (2) \\ &=: c_1\mathcal{U} + c_2\mathcal{U}_{tt} + c_3|\mathcal{U}|^2\mathcal{U} + c_4|\mathcal{U}|^4\mathcal{U} =: F(\mathcal{U}, \phi). \end{aligned}$$

Here, the c_i are complex coefficients. In contrast to the case of soliton solutions of the NLS equation, the constant phase, ϕ , is not a free parameter in Eq. (2), but must rather be solved for simultaneously with the complex envelope, \mathcal{U} [5, 8]. As we will explain in Section 2.4, we search for stationary solutions, $\mathcal{U}(t, z) = U(t)$, of Eq. (2) by using a Newton-type method to solve the equation $F(U(t), \phi) = 0$.

2.3. The spectrum and stability of a stationary solution

To compute the spectrum and determine the linear stability of a stationary solution, U , we suppose that $\mathcal{U} = U + \varepsilon\Delta U$. Then, the order- ε perturbation, ΔU , satisfies

$$\begin{aligned} \Delta U_z &= [c_1 + c_2\partial_t^2 + 2c_3|U|^2 + 3c_4|U|^4] \Delta U + [c_3U^2 + 2c_4|U|^2U^2] \Delta U^* \\ &=: M_1\Delta U + M_2\Delta U^*, \end{aligned} \quad (3)$$

where U^* denotes the complex conjugate of U . If we set $\Delta U(z, t) = e^{\lambda z} v(t) + e^{\lambda^* z} w^*(t)$, and make use of the linear independence of the functions $e^{\lambda z}$ and $e^{\lambda^* z}$, we find that [9]

$$\lambda \begin{bmatrix} v \\ w \end{bmatrix} = \begin{bmatrix} M_1 & M_2 \\ M_2^* & M_1^* \end{bmatrix} \begin{bmatrix} v \\ w \end{bmatrix} =: \mathbf{M}\mathbf{v}. \quad (4)$$

The linear stability of stationary solutions of Eq. (2) is therefore determined by the spectrum of the operator \mathbf{M} . The eigenvalues of \mathbf{M}

come in complex conjugate pairs since $\mathbf{N} = \mathbf{W}^* \mathbf{M} \mathbf{W}$ has real entries, where $\mathbf{W} = \frac{1}{\sqrt{2}} \begin{bmatrix} 1 & 1 \\ i & -i \end{bmatrix}$ is unitary. In particular, the operator, \mathbf{M} , has two branches of continuous spectrum [3], $\{\lambda_c, \lambda_c^*\}$ where

$$\lambda_c = \lambda_c(\omega) = c_1 - c_2 \omega^2 = \delta - \beta \omega^2 + i \left(\phi + \frac{D}{2} \omega^2 \right). \quad (5)$$

Since we have assumed that $\delta < 0$ and $\beta > 0$, the continuous spectrum is always stable. In the next section, we describe the method that we used to numerically compute the discrete spectrum.

2.4. Computational implementation

In this section, we describe the computational methods we used to obtain a parameterized family of stationary solutions of Eq. (2) and to determine how the spectrum of the solution evolves as the parameters in the equation vary. These methods are somewhat simpler versions of methods developed by Wang et al. [8]. However, the problem we solve is also fundamentally simpler, since the equations involved are all local in time, whereas those in [8] include nonlocal terms due to the slow saturation of the gain in the Haus mode-locking equation.

For simplicity, we consider the case that the dispersion coefficient, D , varies over a regular grid of points $D_n = D_0 + n\Delta D$, with all other parameters held constant. We discretize the ordinary differential equation, $F(U, \phi) = 0$, for the stationary solution and the stability eigenproblem, $\mathbf{M}\mathbf{v} = \lambda\mathbf{v}$, using a finite time window, $[-L, L]$, and a seven-point centered difference for the second derivative operator, ∂_t^2 [8]. Specifically, we set $t_k = -L + (k-1)\Delta t$ for $k = 1, \dots, K$, and for any function u on $[-L, L]$ we let $u_k := u(t_k)$. Then, the seven-point second difference operator is given by

$$\begin{aligned} (\partial_t^2 u)_k &= \frac{1}{(\Delta t)^2} [c_0 u_k + c_1 (u_{k-1} + u_{k+1}) \\ &\quad + c_2 (u_{k-2} + u_{k+2}) + c_3 (u_{k-3} + u_{k+3})], \end{aligned} \quad (6)$$

where $c_0 = -49/18$, $c_1 = 1.5$, $c_2 = -0.15$, and $c_3 = 1/90$. This discretization of the second derivative operator is fifth-order accurate.¹ We note that the computation of $(\partial_t^2 u)_k$ for $k \in \{1, 2, 3, K-2, K-1, K\}$ requires values of u_ℓ for $\ell \in \{-2, -1, 0, K+1, K+2, K+3\}$, which are unknown. Since we are searching for bright soliton solutions of Eq. (1) that are rapidly decaying in time, for the problem of finding stationary solutions, $U = U(t)$, we may assume that U is zero outside the time window, $[-L, L]$. However,

¹For a limited set of system parameters, we verified that a three-point central difference scheme works just as well.

as we will explain below, this assumption is not necessarily valid for the computation of the spectrum of \mathbf{M} .

To determine stationary solutions, we formulate the problem of solving for $\mathbf{U} = [U_1, \dots, U_K]$ and ϕ in $F(\mathbf{U}, \phi) = 0$ as a nonlinear least squares problem, which we solve using the Newton-type Levenberg–Marquardt algorithm [17]. For the first dispersion value, D_0 , we obtain an initial guess, $(\mathbf{U}_0^{(0)}, \phi_0^{(0)})$, for the Levenberg–Marquardt algorithm by numerically solving Eq. (1) over a long distance with a Gaussian pulse as the initial condition. For subsequent dispersion values, D_n , we obtain an initial guess, $(\mathbf{U}_n^{(0)}, \phi_n^{(0)})$ using the stationary solution, $(\mathbf{U}_{n-1}, \phi_{n-1})$, obtained for the previous dispersion value, D_{n-1} . In this way, we obtain a family of stationary bright soliton solutions of the CQ-CGL equation (1).

We use the following method to compute the discrete spectrum of the linearized operator, \mathbf{M} . For discrete eigenvalues that correspond to rapidly decaying eigenfunctions the method is fairly standard, since in the computation of the second difference matrix we may assume that the eigenfunctions are zero outside the time window, $[-L, L]$. However, for discrete eigenvalues that are close to the continuous spectrum, the eigenfunctions may decay slowly as $t \rightarrow \pm\infty$. Consequently, the use of zero or periodic boundary conditions on a finite time window can result in large errors in the computed spectrum. In particular, with such boundary conditions it is not possible in practice to observe whether or not discrete eigenvalues merge into or emerge from the continuous spectrum as the parameters in the equation vary. To solve this problem, we modify the action of the second derivative operator using the decay rate of the eigenfunction near $t = \pm L$. Since this decay rate itself depends on the eigenvalue, λ , this procedure results in a nonlinear eigenproblem of the form, $\mathbf{M}(\lambda)\mathbf{v} = \lambda\mathbf{v}$, which we solve using a fixed-point iteration.

To simplify notation, when $D = D_n$, we let λ_n denote one of the discrete eigenvalues, and we let $\lambda_n^{(s)} \rightarrow \lambda_n$ be the sequence of approximations to λ_n obtained using the fixed-point iteration. For $D = D_0$, we first compute an initial estimate of the spectrum using zero boundary conditions in the second difference matrix. By choosing the initial dispersion, D_0 , so that the discrete and continuous eigenvalues are well separated in the complex plane, we can manually identify each point, $\lambda_0^{(0)}$, in the discrete spectrum. When $D = D_n$, for $n > 0$, we instead obtain an initial estimate, $\lambda_n^{(0)}$, for a given discrete eigenvalue, λ_n , using the formula

$$\lambda_n^{(0)} = \lambda_{n-1} + \lambda'(D_{n-1})\Delta D, \quad (7)$$

where λ_{n-1} is a discrete eigenvalue we previously computed for $D = D_{n-1}$, and where for $n > 1$ we estimate the derivative using the backward difference $\lambda'(D_{n-1}) \approx (\lambda_{n-1} - \lambda_{n-2})/\Delta D$. (For $n = 1$ we use $\lambda'(D_0) = 0$.)

For a given dispersion value, D_n , once we have an initial estimate, $\lambda_n^{(0)}$, for a particular discrete eigenvalue, we use an iterative procedure to obtain a sequence of refinements, $\lambda_n^{(s)}$, which we stop when $|\lambda_n^{(s)} - \lambda_n^{(s-1)}|$ is sufficiently small. Within each iteration, we use the current estimate, $\lambda_n^{(s-1)}$, of the eigenvalue to determine the decay rate of the corresponding eigenfunction, $[v, w]^T$, near $t = \pm L$. This decay rate is then used to estimate the unknown values, v_ℓ and w_ℓ for $\ell \in \{-2, -1, 0, K + 1, K + 2, K + 3\}$, in the second difference operator given in Eq. (6). Specifically, since we may assume that $U = 0$ near $t = \pm L$, the eigenfunction, $[v, w]^T$, in Eq. (3) satisfies

$$\partial_t^2 v = \frac{\lambda_n^{(s-1)} - c_1}{c_2} v \quad \text{and} \quad \partial_t^2 w = \frac{\lambda_n^{(s-1)} - c_1^*}{c_2^*} w. \quad (8)$$

Focusing attention on v , let $\eta^2 = [\lambda_n^{(s-1)} - c_1]/c_2$ where $\Re(\eta) > 0$. Then, since the amplitude of the eigenfunction should decay as $t \rightarrow \pm\infty$, we conclude that $v(t) = \alpha_1 e^{\eta t}$ near $t = -L$ and $v(t) = \alpha_2 e^{-\eta t}$ near $t = L$, for some constants α_j . Using this functional form for v , we can solve for the unknown components, v_ℓ with $\ell \in \{-2, -1, 0, K + 1, K + 2, K + 3\}$, in Eq. (6) in terms of v_1 and v_K (and similarly for w). For example, when $\ell \in \{-2, -1, 0\}$, we have that $v_\ell = v_1 \exp[(\ell - 1)\eta t]$. In this manner, we obtain an improved estimate for the second difference operator in Eq. (6) and hence for the linearized operator, $\mathbf{M} = \mathbf{M}[\lambda_n^{(s-1)}]$, which now depends on our current estimate, $\lambda_n^{(s-1)}$, of the discrete eigenvalue, λ_n . Finally, to solve the nonlinear eigenproblem, $\mathbf{M}(\lambda)\mathbf{v} = \lambda\mathbf{v}$, we use the fixed-point iteration

$$\mathbf{M}[\lambda_n^{(s-1)}]\mathbf{v}_n^{(s)} = \lambda_n^{(s)}\mathbf{v}_n^{(s)} \quad (9)$$

to determine the eigenvalue $\lambda_n^{(s)}$ of $\mathbf{M}[\lambda_n^{(s-1)}]$ that is closest to $\lambda_n^{(s-1)}$.

3. Small dissipation results at an edge bifurcation

In this section, we study the performance of our computational method by tracking a discrete eigenvalue of the perturbed NLS equations as it moves into the continuous spectrum in an edge bifurcation. We compare our results to those obtained via an analytical Evans function calculation of Kapitula and Sandstede [2, 11]. Following [11], we introduce a small parameter, $\alpha > 0$, and choose the parameters in the CQ-CGL equation (1) to be $D = 2, \gamma = 4, \nu = 3\alpha, \delta = 0, \beta = \alpha, \epsilon = 8\alpha$, and $\mu = -\alpha$. Using soliton perturbation theory, Kapitula and Sandstede [11, eq. (6)] derived a stationary

solution of the form

$$u(t, z) = \sqrt{\frac{\phi_0}{2}} \operatorname{sech}(\sqrt{\phi_0} t) \exp(i \phi_0 z) [1 + \alpha \Psi(t; \phi_0) + \mathcal{O}(\alpha^2)], \quad (10)$$

where the constant ϕ_0 is independent of α and the function Ψ is independent of z . For the parameters we used, $\phi_0 = 17.5$.

We first used our method to continue the stationary solution $u(t, z) = U(t) \exp(i \phi z)$ from the solution given by (10) at $\alpha = 0$ out to $\alpha = 0.01$. At $\alpha = 0.01$, the eigenfunction corresponding to the discrete eigenvalue, $\lambda(\alpha)$, that is closest to the edge, λ_e , of the continuous spectrum was reasonably well localized, and could be well approximated with the aid of a standard eigenvalue solver by using zero boundary conditions in the second difference matrix. We were then able to successfully continue the pair, (U, ϕ) , and the discrete eigenvalue, $\lambda(\alpha)$, back from $\alpha = 0.01$ to $\alpha = 2 \times 10^{-4}$, at which point $|\lambda(\alpha) - \lambda_e| = 1.4 \times 10^{-6}$. Using a regression algorithm, we obtained the linear fit, $\phi \approx 17.5 + 59.95 \alpha$, for the phase with a 95% confidence interval, [59.87, 60.01], for the slope. However, when we held $\phi = \phi_0$ fixed and just solved for U , we found that the residual output by the Levenberg–Marquardt algorithm exceeded the tolerance we imposed, and the algorithm failed to find a stationary solution. These results highlight how important it is for analytical studies of perturbed nonlinear wave equations to use a pulse ansatz in which the phase is not constant [2, 3, 11], but rather depends on the perturbation parameter.

Starting with the constant phase ansatz in Eq. (10), Kapitula and Sandstede [11, eq. (21)] proved that the discrete eigenvalue, $\lambda(\alpha)$, that bifurcates out of the edge, $\lambda_e = i \phi_0$, of the continuous spectrum satisfies

$$\lambda(\alpha) - \lambda_e = -\frac{A \phi_0^2}{18} \alpha^2 + i \phi_0 \frac{A^2 - \phi_0^2}{36} \alpha^2 + \mathcal{O}(\alpha^3), \quad (11)$$

where, for the parameters we used, $A = -15.5$. Although Eq. (11) was derived under the assumption of a constant phase, $\phi = \phi_0$, the results shown in Fig. 1 strongly suggest that (11) also holds if we assume that $\phi = \phi_0 + m \alpha$, provided that we set $\lambda_e = i(\phi_0 + m \alpha)$, as suggested by Eq. (5). Indeed it should be possible to adapt the proof of (11) given in [2, 11] to establish this more general and physically meaningful result. In the left panel (respectively, center panel) of Fig. 1 we plot the real part (respectively, imaginary part) of the eigenvalue as a function of the small parameter, α . The results obtained using our method are shown with the blue solid line, and the results obtained using Eq. (11) are shown with the red dashed line. In the right panel, we show that the error between the two methods is $\mathcal{O}(\alpha^3)$, as predicted by the theory.

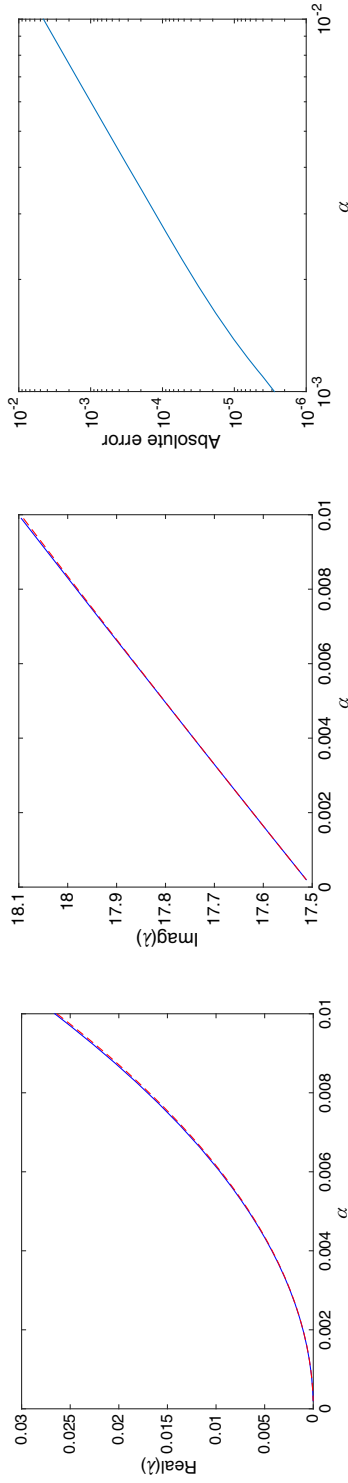


Figure 1. Small dissipation results at an edge bifurcation. Left: The real part of the bifurcating eigenvalue as a function of α . The results obtained using our method are shown with the blue solid line, and the results obtained using Eq. (11) with $\lambda_e = i(\phi_0 + m\alpha)$ are shown with the red dashed line. Center: The imaginary part of the same eigenvalue. Right: The distance between the eigenvalues obtained using the two methods.

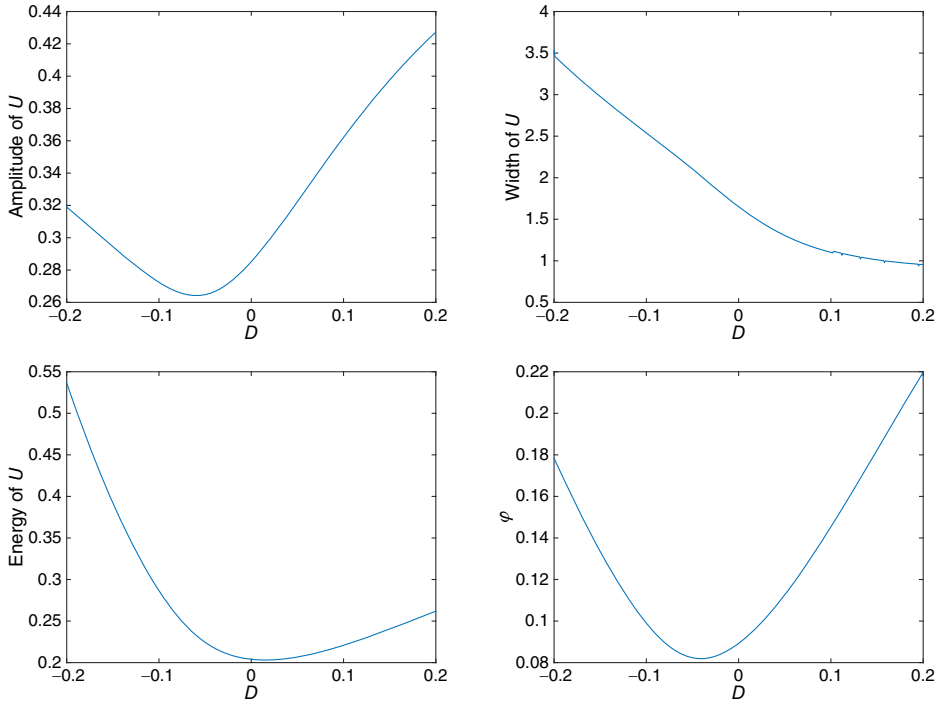


Figure 2. Amplitude, width, energy, and ϕ -parameter of the stationary solution as functions of dispersion, D .

4. Large dissipation results across zero dispersion

4.1. Stationary solutions

To study short pulse solutions in the vicinity of zero dispersion, we varied the dispersion from $D = -0.2$ to $D = 0.2$ and fixed the other parameters in the CGL equation (1) to be $\delta = -0.01$, $\beta = 0.08$, $\gamma = 1$, $\epsilon = 1$, $\nu = 10$, and $\mu = -3$. The stationary pulses we found using the Newton-type method are similar to those found by Soto-Crespo et al. [5] for a different set of parameters using a numerical PDE solver. In Fig. 2, we plot the pulse parameters as a function of the dispersion, D . We show the amplitude and width of the pulse in the upper left and upper right panels, respectively, and the pulse energy and the phase parameter ϕ in the stationary solution, $u(t, z) = U(t)e^{i\phi z}$ of Eq. (1), in the lower left and lower right panels, respectively. We define the width of the pulse to be the full-width at half-maximum of the pulse amplitude and the pulse energy to be $E = \int |U(t)|^2 dt$. These results are in qualitative agreement with results obtained by Soto-Crespo et al. [5] for a similar set of parameters. The most important feature in these plots is the significant narrowing of the pulse

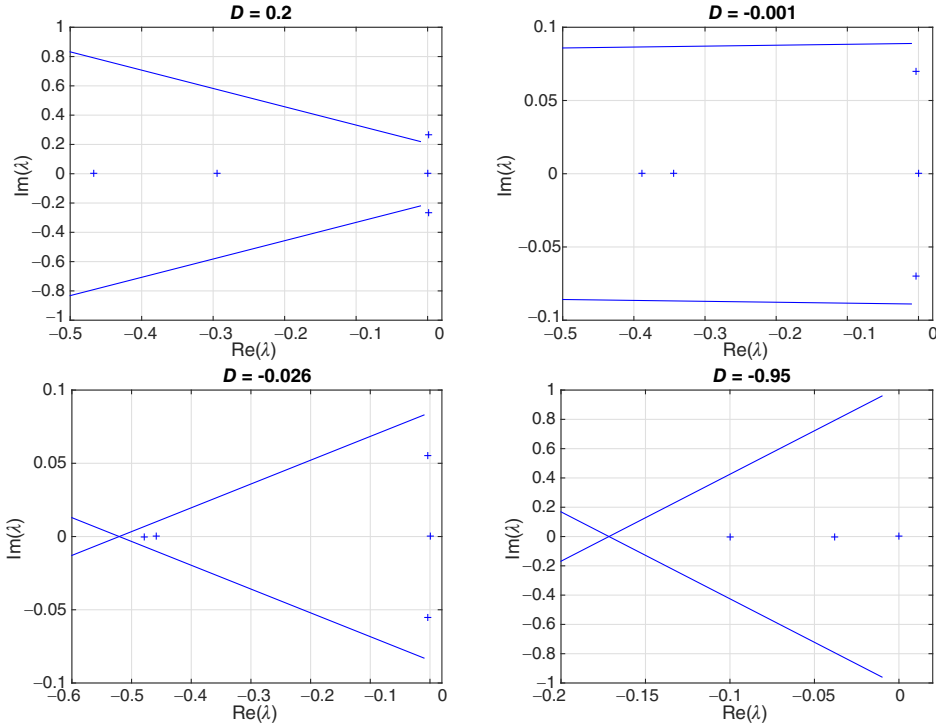


Figure 3. Spectrum of the stationary solutions for $D = 0.2$ (upper left), $D = -0.001$ (upper right), $D = -0.026$ (lower left), and $D = -0.95$ (lower right).

as the dispersion increases from the normal to the anomalous dispersion regime.

4.2. Linear stability and pulse spectrum

Although the narrowing of the pulse width is the only significant change in the stationary solution as the dispersion changes from normal to anomalous, we will now show that there are several significant changes in the pulse spectrum in the complex plane. Moreover, as we will see, the structure of these spectra can be quite different from that of the hyperbolic secant solution of the NLS equations, for which the continuous spectrum is a pair of half-lines on the positive and negative imaginary axes with edges at $\pm i\phi$, and the discrete spectrum consists of a single eigenvalue of algebraic multiplicity four at the origin [18].

In Fig. 3, we plot the spectrum of the stationary solutions found in Section 4.1 for $D = 0.2$ (upper left), $D = -0.001$ (upper right), $D = -0.026$ (lower left), and $D = -0.95$ (lower right). We note that the scales differ in each of these plots. For each value of the dispersion parameter,

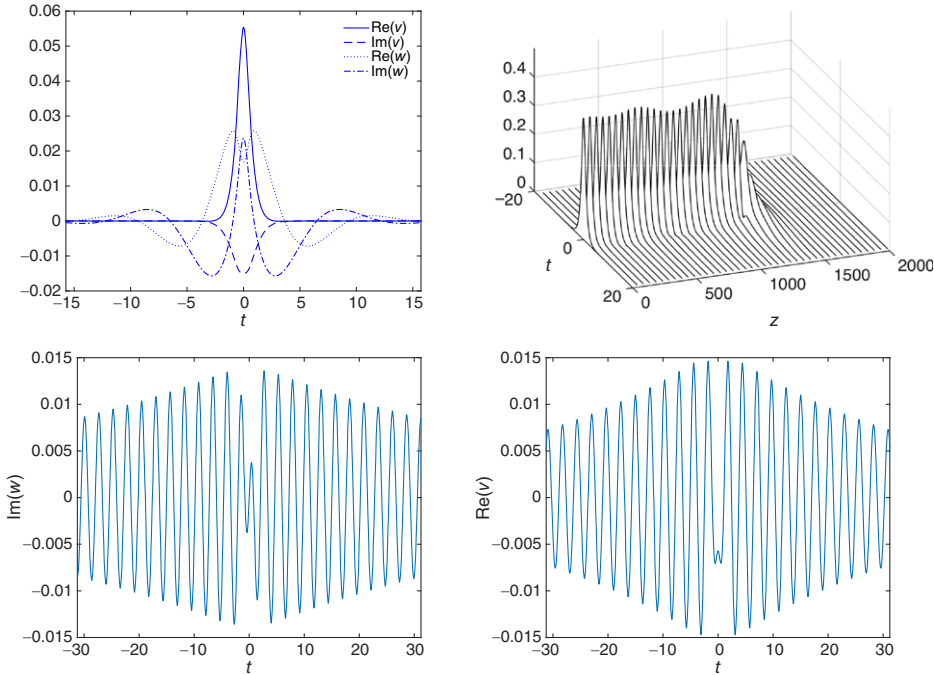


Figure 4. Upper Left: The eigenfunction of the unstable eigenvalue, λ_+ , when $D = 0.2$. Upper right: Evolution of a perturbation of the stationary solution by the unstable eigenfunction in the upper left panel. Lower left: The imaginary part of the w -component of the eigenfunction with eigenvalue, $\lambda_{\mathfrak{N},2}$, when $D = -0.026$. Lower right: The real part of the v -component of the eigenfunction with eigenvalue, $\lambda_{\mathfrak{N},1}$, when $D = -0.026$.

D , we obtained the continuous spectrum using Eq. (5) together with the computed values for the phase, ϕ , shown in the bottom right panel of Fig. 2. For all values of D , the continuous spectrum is a pair of complex conjugate half-lines in the left-half plane with edges at the points $\delta \pm i\phi$. As we see in the lower right panel of Fig. 2, the phase $\phi > 0$ for all the stationary solutions we studied. Consequently, by Eq. (5), when $D > 0$ the two branches of the continuous spectrum slope toward the origin but do not intersect (as in the upper left panel of Fig. 3). In particular, there is a band gap between $\delta \pm i\phi$, as in the case of the NLS equation [18]. In the special case that $D = 0$, the continuous spectrum forms a complex conjugate pair of half-lines parallel to the real axis. (The upper right panel shows the $D = -0.001$ perturbation of this case.) Finally, when $D < 0$ the band gap disappears and the two branches of the continuous spectrum intersect at the point $x(D) = \delta + 2\beta\phi/D$ on the negative real axis (as in the lower two panels of Fig. 3). We note that $x(D) \rightarrow -\infty$ as $D \rightarrow 0^-$.

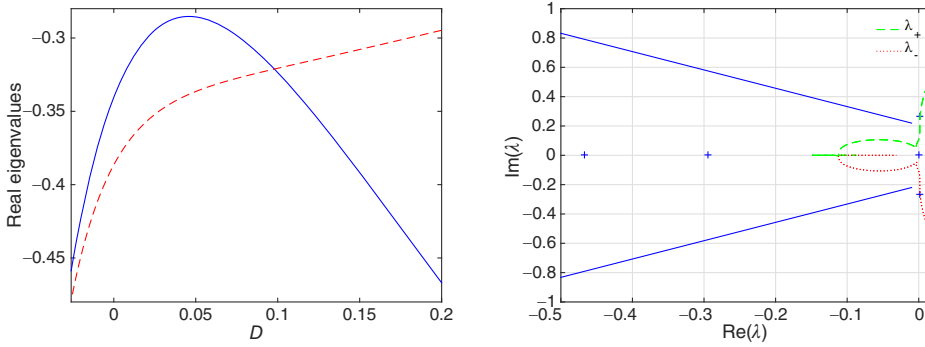


Figure 5. Left: The real eigenvalues, $\lambda_{\Re,1}$ (solid blue line) and $\lambda_{\Re,2}$ (dashed red line), as functions of D . Right: The curves of the eigenvalues, λ_+ (dashed green curve) and λ_- (dotted red curve), parameterized by D which decreases from $D = 0.2$ to $D = -1$. The curves start in the right-half plane at $D = 0.2$. The solid blue lines and symbols show the spectrum at the Hopf bifurcation point, $D_{\text{cr}} = 0.047$.

We now discuss how the structure of the discrete spectrum changes as the dispersion changes from the anomalous to the normal regime. We computed each of the discrete eigenvalues using the method described in Section 2.4. We verified that if we simultaneously double the computational time window and quadruple the number of grid points, that the results shown in Figures 3 and 5 do not change. In particular, the maximum over all dispersion values of the absolute error between the eigenvalues computed using the two sets of discretization parameters was 1.9×10^{-5} .

For all dispersion values, there is a double eigenvalue at zero, due to the phase and translational invariance of Eq. (1). In addition, for $D = 0.2$ (see the upper left panel of Fig. 3) there are four more discrete eigenvalues: a complex conjugate pair of eigenvalues, $\lambda_{\pm} = 0.00195 \pm 0.2666i$, located near the edge of the continuous spectrum, and two eigenvalues, $\lambda_{\Re,1} = -0.4669$ and $\lambda_{\Re,2} = -0.2947$, on the negative real axis. We observe that for $D = 0.2$ the stationary solution is unstable since $\Re(\lambda_{\pm}) > 0$. This spectrum is in qualitative agreement with that shown in Wang et al. [8, fig. 3], for a different set of parameters in the anomalous regime, except that the unstable eigenvalues, λ_{\pm} , are not present, and so there are only four discrete eigenvalues in their spectrum.

In the upper left panel of Fig. 4, for $D = 0.2$, we plot the real and imaginary parts of the components, v and w , of the unstable eigenfunction with eigenvalue, λ_+ . As we see in the upper right panel of Fig. 4, if we perturb the stationary solution, U , using a scaling of this unstable eigenfunction whose amplitude is 1% of the amplitude of U , we find that the amplitude of the pulse first oscillates in z , before eventually dissipating to the zero solution.

Returning our attention to Fig. 3, we observe that when $D = 0.2$, the eigenvalue, λ_+ , lies slightly above the edge of the upper branch of the continuous spectrum, whereas for $D = -0.001$ it lies below. For intermediate values of D , we observed that although the eigenvalues, λ_{\pm} , come close to the continuous spectrum they do not merge with it. In fact the corresponding eigenfunctions decay with sufficient rapidity that the values computed for λ_{\pm} when we use decaying boundary conditions for the second difference operator agree very well with those obtained using zero boundary conditions. Once D has decreased to $D = -0.001$ (upper right panel), the eigenvalues, λ_{\pm} , have moved into the left-half plane, the eigenvalues $\lambda_{\Re,1}$ and $\lambda_{\Re,2}$ are still on the negative real axis, and the pulse is stable. For $D = -0.026$ (lower left panel), the spectrum agrees qualitatively with that shown in Akhmediev et al. [9, fig. 2], for a different set of parameters in the normal dispersion regime, except that the two negative real eigenvalues, $\lambda_{\Re,1}$ and $\lambda_{\Re,2}$, are not present, and so there are only four discrete eigenvalues in their spectrum. All the results we have shown so far are in qualitative agreement with the small dissipation theory of Kapitula [3] and Kapitula and Sandstede [2].

We now recall the analytical result of Kapitula and Sandstede [2] for the PCQ-NLS equation that if a discrete eigenvalue merges into the continuous spectrum it does so only at the edge, $\delta \pm i\phi$. In contrast to this result, we will now show that in the normal dispersion regime when the dissipative parameters in Eq. (1) are no longer small, the pair of negative real eigenvalues, $\lambda_{\Re,1}$ and $\lambda_{\Re,2}$, can simultaneously merge into the intersection point of the two branches of the continuous spectrum. First, we see in the lower left panel of Fig. 3 that as D decreases below zero, the intersection point of the two branches of the continuum approaches the real eigenvalues, $\lambda_{\Re,1}$ and $\lambda_{\Re,2}$. In fact, for $D = -0.026$, these two eigenvalues are sufficiently close to the continuous spectrum that the corresponding eigenfunctions decay slowly as $t \rightarrow \pm\infty$. For example, in the lower panels of Fig. 4, we plot two components of the eigenvectors with eigenvalues $\lambda_{\Re,2} = -0.4789$ (left) and $\lambda_{\Re,1} = -0.4588$ (right).

In the left panel of Fig. 5, we plot the real eigenvalues, $\lambda_{\Re,1}$ with a solid blue line and $\lambda_{\Re,2}$ with a dashed red line, as functions of D . As D decreases from $D = 0.2$, $\lambda_{\Re,2}$ decreases and merges with the intersection point of the two branches of the continuous spectrum at $D \approx -0.03$. At the same time, $\lambda_{\Re,1}$ first increases and then decreases, merging into the intersection point of the two branches of the continuous spectrum at the same dispersion value. At least for $-1 < D < -0.03$, there are only four discrete eigenvalues, instead of the original six.

Finally, in the right panel of Fig. 5, we track the evolution of the eigenvalues, λ_{\pm} , as D decreases from $D = 0.2$ to $D = -1$. The path taken by λ_+ is shown with the dashed green curve and that taken by λ_- is shown

with the dotted red curve. At $D = 0.2$, the eigenvalue, λ_+ , is located at the top right point on the dashed green curve. As D decreases, λ_+ moves down the dashed green curve, crossing into the left-half plane at $D_{\text{cr}} = 0.047$ at which point the pulse becomes stable. Therefore, there will be a periodic solution at this Hopf bifurcation. The spectrum shown with solid blue lines and symbols in Fig. 5 is the spectrum of the pulse at D_{cr} . When we decrease D below the value $D \approx -0.03$ at which the real eigenvalues, $\lambda_{\mathfrak{R},1}$ and $\lambda_{\mathfrak{R},2}$ merge with the continuous spectrum, the complex eigenvalues, λ_{\pm} , collide on the negative real axis. After the collision, one eigenvalue (shown with the dotted red line) moves to the right on the real axis and the other eigenvalue (shown with the dashed green line) moves first to the left and then to the right. We have not been able to continue the stationary solution far enough into the region $D < -1$ to determine whether the pulse becomes unstable again.

5. Comparison with computational Evans function methods

In this section, we compare the method we used to determine discrete eigenvalues of the linearized problem to computational methods based on the Evans function [13–16]. We computed the eigenvalues by using general-purpose numerical linear algebra software to solve a nonlinear eigenvalue problem using a fixed-point iteration. The nonlinearity of this eigenvalue problem arises because the boundary conditions imposed for the discretization of the second derivative operator, ∂_t^2 , depend on the exponential decay rate of the eigenfunction, and hence on the eigenvalue we wish to compute. The idea of using exact asymptotic boundary conditions at the ends of the computational time window also forms the basis of the computational Evans methods [15].

Building on prior work by Pego and Weinstein [10, 13] for a KdV–Burgers equation, Afendikov and Bridges [14] developed a computational Evans function method for the cubic CGL equation. The discrete eigenvalues are those $\lambda \in \mathbb{C}$ for which there is a nontrivial solution to an associated first-order system of ordinary differential equations of the form

$$\mathbf{v}_t = \mathbf{A}(t; \lambda) \mathbf{v} \quad \text{for } \mathbf{v} = \mathbf{v}(t) \in \mathbb{C}^4, \quad (12)$$

with $\mathbf{v}(\pm\infty) = 0$. The spectrum of the constant coefficient operator $\mathbf{A}(\lambda) := \lim_{t \rightarrow \pm\infty} \mathbf{A}(t; \lambda)$ has two eigenvalues with a positive real part and two with a negative real part, which depend analytically on λ away from the continuous spectrum. Let $U_-(t; \lambda)$ (respectively, $S_+(t; \lambda)$) be the two-dimensional unstable (respectively, stable) manifold of solutions whose exponential decay rates as $t \rightarrow -\infty$ (respectively, $t \rightarrow +\infty$) are given

by the two eigenvalues with positive (respectively, negative) real part. If $\mathbf{W}_-(t; \lambda)$ (respectively, $\mathbf{W}_+(t; \lambda)$) is a 4×2 matrix whose columns form an analytically varying basis for $U_-(t; \lambda)$ (respectively, $S_+(t; \lambda)$), then the Evans function is the analytic function $\mathcal{D}(\lambda) = \det[\mathbf{W}_-(t; \lambda) \ \mathbf{W}_+(t; \lambda)]$. Since λ is an eigenvalue if and only if $U(t; \lambda) \cap S(t; \lambda) \neq \emptyset$, the eigenvalues are the zeros of \mathcal{D} .

Because the two basis vectors for $U_-(t; \lambda)$ (or $S_+(t; \lambda)$) have different growth rates, the problem of computing pairs of linearly independent solutions of Eq. (12) is stiff, and so the numerically computed basis vectors will not maintain linear independence. To overcome this stiffness problem, rather than solving for the basis vectors individually, Afendikov and Bridges [14] regard $\mathbf{W}_\pm(t; \lambda)$ as being an element of the six-dimensional exterior-product vector space, $\Lambda^2(\mathbb{C}^4)$, and formulate a 6×6 system of first-order equations for \mathbf{W}_\pm which can be solved numerically using standard techniques. The resulting algorithm for computing the Evans function is both fast and robust. Afendikov and Bridges then used a Newton solver to compute the zeros of \mathcal{D} in the right-half plane. Because the Evans function is complex analytic, generalizations of the Argument Principle have also been used to find the zeros of \mathcal{D} via numerical computation of certain contour integrals [13, 15]. More recently, Humpherys and Lytle [16] developed a root-following method to track an eigenvalue, λ , as a parameter in the equation varies. This method, which is formulated as a two-point boundary value problem for $(\mathbf{W}_-, \mathbf{W}_+, \lambda)$, is somewhat more efficient than the contour integration methods. However, because the domain of analyticity of \mathcal{D} must avoid the continuous spectrum, to our knowledge computational Evans function methods have not yet been applied to the problem addressed in this paper of tracking eigenvalues as they merge with or emerge from the continuous spectrum. This observation is somewhat surprising, as it is precisely in this situation that the standard numerical methods for computing eigenvalues fail. An important open problem is to develop robust computational methods to determine the stability of periodically stationary solutions of the nonlocal equations that model realistic laser systems, including those that have been shown to generate flat-topped pulse shapes [19, 20]. Two promising approaches are based on the methods used for the results in this paper and on more recent theoretical and computational Evans function methods [12, 16].

6. Conclusions

We described computational methods to compute variations in the spectra of stationary solutions of the CQ-CGL equation as the coefficients in the equation vary. In the anomalous dispersion regime, the spectra we obtained

in the presence of large dissipative effects are in qualitative agreement with the theoretical results of Kapitula and Sandstede obtained for $O(\varepsilon)$ -perturbations of the CQ-NLS equation [2, 3]. However, after the dispersion crosses zero into the normal dispersion regime, we observed variations in the spectrum due to large dissipative effects that are not predicted by the small dissipation, PCQ-NLS theory.

Our original motivation for investigating the stability of pulse solutions of the CQ-CGL equation near zero dispersion was that results of Gordon and Haus [21] for the NLS equation suggest that timing and phase jitter should be minimized when the average dispersion in the laser cavity is close to zero. Indeed, this phenomenon has recently been observed in experiments [22]. The methods we have described here will be used to develop fully numerical methods to compute the effects of noise in short pulse lasers modeled by generalizations of the CGL equation.

References

1. J. N. KUTZ, Mode-locked soliton lasers, *SIAM Rev.* 48:629–678 (2006).
2. T. KAPITULA and B. SANDSTEDE, Stability of bright solitary-wave solutions to perturbed nonlinear Schrödinger equations, *Physica D* 124:58–103 (1998).
3. T. KAPITULA, Stability criterion for bright solitary waves of the perturbed cubic-quintic Schrödinger equation, *Physica D* 116:95–120 (1998).
4. Y. SHEN, P. G. KEVREKIDIS, N. WHITAKER, N. I. KARACHALIOS, and D. J. FRANTZESKAKIS, Finite-temperature dynamics of matter-wave dark solitons in linear and periodic potentials: An example of an anti-damped Josephson junction, *Phys. Rev. A* 86:033616–033628 (2012).
5. J. M. SOTO-CRESPO, N. N. AKHMEDIEV, V. V. AFANASJEV, and S. WABNITZ, Pulse solutions of the cubic-quintic complex Ginzburg–Landau equation in the case of normal dispersion, *Phys. Rev. E* 55:4783–4796 (1997).
6. N. AKHMEDIEV, J. M. SOTO-CRESPO, and P. GRELU, Roadmap to ultra-short record high-energy pulses out of laser oscillators, *Phys. Lett. A* 372:3124–3128 (2008).
7. J. M. SOTO-CRESPO, N. N. AKHMEDIEV, and V. V. AFANASJEV, Stability of the pulselike solutions of the quintic complex Ginzburg Landau equation, *J. Opt. Soc. Am. B* 13:1439–1449 (1996).
8. S. WANG, A. DOCHERTY, B. S. MARKS, and C. R. MENYUK, Boundary tracking algorithms for determining the stability of mode-locked pulses, *J. Opt. Soc. Am. B* 31:2914–2930 (2014).
9. N. AKHMEDIEV and J. M. SOTO-CRESPO, Exploding solitons and Shil’nikov’s theorem, *Phys. Lett. A* 317:287–292 (2003).
10. R. L. PEGO and M. I. WEINSTEIN, Eigenvalues, and instabilities of solitary waves, *Philos. Trans. R. Soc. Lond. A* 340:47–94 (1992).
11. T. KAPITULA and B. SANDSTEDE, Instability mechanism for bright solitary-wave solutions to the cubic–quintic Ginzburg–Landau equation, *J. Opt. Soc. Am. B* 15:2757–2762 (1998).
12. T. KAPITULA, N. KUTZ, and B. SANDSTEDE, The Evans function for nonlocal equations, *Indiana Univ. Math. J.* 53:1095–1126 (2004).

13. R. L. PEGO, P. SMEREKA, and M. I. WEINSTEIN, Oscillatory instability of travelling waves for a KdV–Burgers equation, *Physica D* 67:45–65 (1993).
14. A. L. AFENDIKOV and T. J. BRIDGES, Instability of the Hocking–Stewartson pulse and its implications for three-dimensional Poiseuille flow, *Proc. R. Soc. Lond. A* 457:257–272 (2001).
15. T. J. BRIDGES, G. DERKS, and G. GOTTWALD, Stability and instability of solitary waves of the fifth-order KdV equation: A numerical framework, *Physica D* 172:190–216 (2002).
16. J. HUMPHERYS and J. LYTLE, Root following in Evans function computation, *SIAM J. Numer. Anal.* 53:2329–2346 (2015).
17. W. H. PRESS, B. P. FLANNERY, S. A. TEUKOLSKY, and W. T. VETTERLING, *Numerical Recipes in C: The Art of Scientific Computing* (2nd ed.), Cambridge University Press, New York, NY USA, 1992.
18. D. KAUP, Perturbation theory for solitons in optical fibers, *Phys. Rev. A* 42:5689–5694 (1990).
19. W. H. RENNINGER, A. CHONG, and F. W. WISE, Amplifier similaritons in a dispersion-mapped fiber laser [invited], *Opt. Express* 19:22496–22501 (2011).
20. L. NUGENT-GLANDORF, T. A. JOHNSON, Y. KOBAYASHI, and S. A. DIDDMANS, Impact of dispersion on amplitude and frequency noise in a Yb-fiber laser comb, *Opt. Lett.* 36:1578–1580 (2011).
21. J. P. GORDON and H. A. HAUS, Random walk of coherently amplified solitons in optical fiber transmission, *Opt. Lett.* 11:665–667 (1986).
22. Y. SONG, C. KIM, K. JUNG, H. KIM, and J. KIM, Timing jitter optimization of mode-locked Yb-fiber lasers toward the attosecond regime, *Opt. Express* 19:14518–14525 (2011).

THE UNIVERSITY OF TEXAS AT DALLAS
UNIVERSITY OF MARYLAND BALTIMORE COUNTY

(Received August 20, 2015)